Synthesis and magnetotransport properties of Bi_2Se_3 nanowires*

Kang Zhang(张亢)[1], Haiyang Pan(潘海洋)[2], Zhongxia Wei(魏仲夏)[2], Minhao Zhang(张敏昊)[1], Fengqi Song(宋风麒)[2], Xuefeng Wang(王学锋)[1,†], and Rong Zhang(张荣)[1]

[1] *National Laboratory of Solid State Microstructures, Collaborative Innovation Center of Advanced Microstructures, School of Electronic Science and Engineering, Nanjing University, Nanjing* 210093, *China*

[2] *National Laboratory of Solid State Microstructures, Collaborative Innovation Center of Advanced Microstructures, School of Physics, Nanjing University, Nanjing* 210093, *China*

(Received 6 April 2017; revised manuscript received 11 May 2017; published online 18 July 2017)

Bi_2Se_3, as a three-dimensional topological insulator, has attracted worldwide attention for its unique surface states which are protected by time-reversal symmetry. Here we report the synthesis and characterization of high-quality single-crystalline Bi_2Se_3 nanowires. Bi_2Se_3 nanowires were synthesized by chemical vapor deposition (CVD) method via gold-catalyzed vapor-liquid-solid (VLS) mechanism. The structure and morphology were characterized by scanning electron microscopy (SEM), transmission electron microscopy (TEM), x-ray photoelectron spectroscopy (XPS), and Raman spectroscopy. In magnetotransport measurements, the Aharonov–Bohm (AB) effect was observed in a nanowire-based nanodevice, suggesting the existence of surface states in Bi_2Se_3 nanowires.

Keywords: topological insulators, nanowires, chemical vapor deposition, Aharonov–Bohm effect

PACS: 61.46.Km,73.43.Qt,73.63.–b **DOI:** 10.1088/1674-1056/26/9/096101

1. Introduction

Topological insulators (TIs) possess a bulk bandgap and gapless surface states protected by time-reversal symmetry, which has been observed directly by angle-resolved photoemission spectroscopy (ARPES).[1–6] By doping magnetic impurities, the surface states would be gapped, resulting in many exotic topological phenomena.[7–12] For example, a quantum anomalous Hall effect (QAHE) was observed in Cr-doped $(Bi,Sb)_2Te_3$ films.[12,13] Bismuth selenide (Bi_2Se_3), which was identified as one of three-dimensional TI materials, has attracted a great deal of attention and been widely studied. Electronic transport experiments were often carried out to study the surface states of TIs.[14–19] However, the surface states were readily buried by the bulk contribution because of the abundant crystal defects.[20,21] One of the solutions is to synthesize nanomaterials with a large surface-to-volume ratio, which can magnify the surface states' contribution ratio in electronic transport experiments.[16,22,23] Besides, nanostructures of TIs are considered as critical materials for spintronic applications and quantum computers.[24,25] Therefore, it is urgently needed to synthesize high-quality Bi_2Se_3 nanostructures. One of the most prominent methods is the chemical vapor deposition (CVD) technique, which has been reported by various groups.[14,16,18,25] Besides, a series of quantum phenomena related to the surface states have been observed in TIs nanostructures prepared by CVD, including weak antilocalization (WAL),[26] Aharonov–Bohm (AB) interference,[14,16] Shubnikov–de Haas (SdH) oscillations,[27–30] and universal conductance fluctuations (UCF).[14,31]

In this work, we have synthesized high-quality Bi_2Se_3 nanowires by a simple CVD approach. Different characterization methods were used to investigate the structural characteristics and verify the high quality of the nanowires, such as scanning electron microscope (SEM), transmission electron microscopy (TEM) with energy dispersive x-ray spectroscopy (EDS), x-ray photoelectron spectroscopy (XPS), and Raman spectroscopy. We also investigated the transport properties of as-grown nanowires by fabricating nanowire-based nanodevices. The measured magnetoresistance of Bi_2Se_3 nanowires under a magnetic field up to 9 T showed the clear WAL effect and AB oscillations.

2. Experiment method

Bi_2Se_3 nanowires were synthesized in a single heat zone tube furnace, and the quartz tube was 70 cm in length and 30 mm in diameter. Bi_2Se_3 powder (99.999%) was used as the precursor, and Bi_2Se_3 nanowires were grown on silicon substrates covered with a 10 nm gold layer as the catalyst via the vapor-liquid-solid (VLS) mechanism. In the growth process, Bi_2Se_3 powder was placed at the central heat zone in a quartz boat, while the Si substrates in another quartz boat were placed downstream in the low-temperature region, which was 9–15 cm away from the source. In order to remove air and water in the quartz tube, the system was pumped and flushed with Ar gas flow several times prior to the growth. Then the temperature was raised to 560 °C in 30 min and main-

*Project supported by the National Key Basic Research Program of China (Grant Nos. 2014CB921103 and 2013CB921103), the National Natural Science Foundation of China (Grant Nos. 11274003 and 91421109), and Collaborative Innovation Center of Solid-State Lighting and Energy-Saving Electronics, China.

†Corresponding author. E-mail: xfwang@nju.edu.cn

© 2017 Chinese Physical Society and IOP Publishing Ltd

tained at 560 °C for 60 min at a constant Ar gas flow rate of 20 sccm as the carrier gas and protective gas. During the whole growth process, the pressure in the tube was kept at 25 Pa. Then the nanowires were transfered onto the surface of clean SiO_2/Si substrates. The single nanowire devices were fabricated by the photolithography technique and standard lift-off processes, in which Ti(5 nm)/Au(70 nm) alloy was evaporated by electron-beam evaporation (EBE). The transport properties of the Bi_2Se_3 nanowire were measured in a Quantum Design PPMS-9 (physical property measurement system).

3. Results and discussion

The morphology of the as-grown Bi_2Se_3 nanostructures was analyzed by SEM images, as shown in Fig. 1. Figure 1(a) shows the nanostructures on the Si substrate, suggesting that most of the synthesized products are straight nanowires with an average length of about 15 μm. It is seen in Fig. 1(a) that there are Au particles at the tip end of most nanowires. Figure 1(b) shows the magnified SEM image of a single Bi_2Se_3 nanowire with a diameter of about 200 nm. The Au tip at the end of the nanowire can be observed obviously, clearly indicating the VLS growth mechanism.[16,26,32] In addition to the nanowires, the strip-shaped Bi_2Se_3 nanoribbons are obtained at the same time, as shown in Fig. 1(c). The nanoribbon shows a width of over 500 nm, and Au is also seen at the tip end of the nanoribbon, also suggesting the VLS growth mechanism of nanoribbon. The EDS spectrum of a single Bi_2Se_3 nanowire is shown in Fig. 1(d), and the quantitative analysis suggests an atomic ratio of Bi/Se close to 1:1, which indicates that there exist Se vacancies in Bi_2Se_3 nanowires. Because of the low formation energy of the native defects,[33] the as-grown crystals of Bi_2Se_3 always accompany a lot of Se vacancies (usually $\sim 10^{19}$ cm^{-3}) that act as electron donors.[20,34] As a result, Bi_2Se_3 usually displays a metallic behavior and the residual bulk carriers hinder the transport studies of the surface states of Bi_2Se_3.

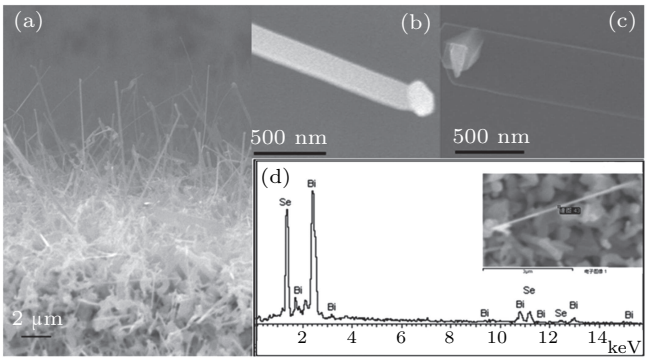


Fig. 1. The SEM images of (a) as-grown Bi_2Se_3 nanowires on substrates, (b) a single nanowire, and (c) a single nanoribbon. (d) The EDS spectrum of a single Bi_2Se_3 nanowire.

In the initial stage of growth, when the furnace temperature was raised to 560 °C, the temperature of the Si substrates was about 350 °C, far below the melting point of Au (1063 °C). In fact, Au is nonreactive but at the nanoscale it becomes a catalyst for reactions.[35–37] The size of Au particle we used is about 5 nm, so the Au particle could melt and form Au droplets on the Si substrates at 350 °C. Then the Au droplets absorb the evaporated Bi_2Se_3 molecules carried by Ar gas flow to form a liquid solution. Along with the increase of dissolved quantity, the solution soon turns to a supersaturated solution and serves as nucleation sites. Further source molecules lead to the Bi_2Se_3 crystallization and the uniaxial growth of Bi_2Se_3 nanowires or nanoribbons. Throughout the entire growth process, it contains three states of matter: vapor (evaporated source), liquid (supersaturated solution), and solid (crystallizing), and it exactly complies with the VLS growth mechanism.[38–40] We notice that the Au particle moves from Si substrates surface to the top of nanowires or nanoribbons during growth, which proves the catalysis of Au in the VLS growth process. However, there should be something different in the detailed growth processes of nanowires and nanoribbons even though they share the same growth mechanism. Compared with thin nanowires, flat nanoribbons like the one shown in Fig. 1(c) indicate the obvious lateral growth, which usually dominates in the absence of a catalyst. It contains three growth processes: evaporation, crystallization, and epitaxial growth. We call this growth mode the vapor-solid (VS) mechanism since there is no liquid substance formed during the whole growth process. We conclude that the formation of nanoribbons includes two mechanisms: uniaxial VLS growth and epitaxial VS growth. When we increase the pressure in the tube or Ar flow rate during growth, the quantity of nanoribbons increases gradually, which is associated with the flow rate of the evaporated source material. Higher pressure or Ar flow rate will increase the mass flow rate of the source material, and VS growth dominates over VLS growth for a large mass flow rate.[38]

Figure 2(a) shows the typical TEM image of a single Bi_2Se_3 nanowire with a width of 150 nm. The good crystallinity of the synthesized nanowire is verified by the high resolution TEM (HRTEM) image shown in Fig. 2(b). The lattice spacing of 0.21 nm in the inset agrees well with the previous reports, indicating that the nanowires grow along the [110] direction.[25,41] The chemical composition of our samples was analyzed by the EDS attached in the TEM. Figure 2(c) shows the EDS spectrum collected from the center of the nanowire, which confirms the compositions of Bi and Se. Further quantitative analysis reveals that the atomic ratio of Bi and Se is about 46:54, also indicating the existence of Se vacancies in Bi_2Se_3 nanowires. The EDS spectrum collected from the head of the short nanowire is shown in Fig. 2(d), suggesting that the particle on the head only contains Au, verifying the VLS growth mechanism. The C and Cu peaks come from the carbon-supported copper grid.

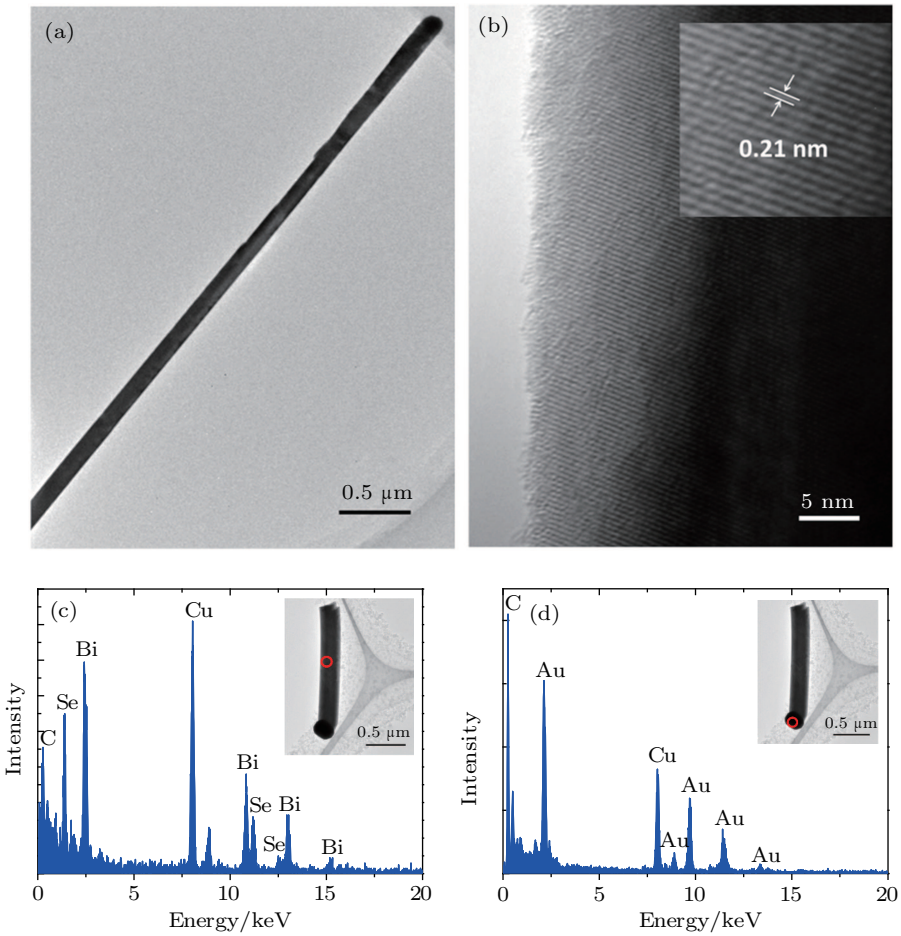


Fig. 2. (color online) (a) TEM and (b) HRTEM images of a typical nanowire. The inset in panel (b) shows the lattice spacing of 0.21 nm. (c), (d) EDS spectra collected from the body and head of a single Bi_2Se_3 nanowire, respectively.

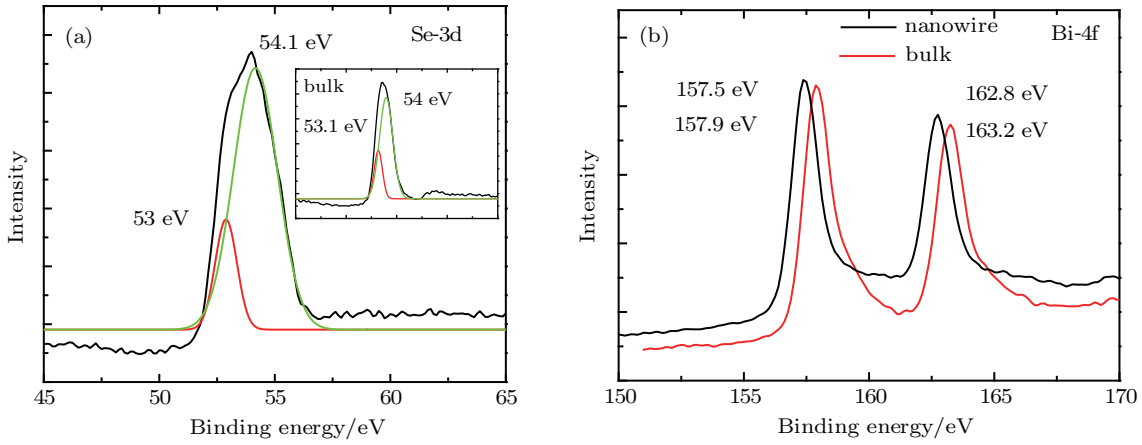


Fig. 3. (color online) XPS spectra of Bi_2Se_3. (a) Se 3d peaks of the nanowires and the bulk (the inset). (b) Bi 4f peaks of the nanowires (black line) and the bulk (red line).

Figure 3(a) shows peaks of Bi_2Se_3 nanowire at 53.0 eV and 54.1 eV that correspond to Se $3d_{5/2}$ and $3d_{3/2}$, respectively, which are consistent with the peaks of bulk Bi_2Se_3 prepared by the melting method at 53.1 eV and 54.0 eV, as shown in the inset. In Fig. 3(b), the black line shows peaks of Bi_2Se_3 nanowire at 157.5 eV and 162.8 eV related to Bi $4f_{5/2}$ and $4f_{7/2}$, which are close to the peaks of bulk Bi_2Se_3 at 157.9 eV and 163.2 eV illustrated by the red line. Compared with the pure bulk of Se and Bi for Bi_2Se_3 nanowires, the binding energies of the Se 3d peaks decrease by about 1.6 eV, while the binding energies of Bi 4f peaks increase by about 0.5 eV. The changes of the binding energies are caused by the Se–Bi bond and the charge transfer from Bi to Se. In Fig. 4, we show a typical Raman spectrum taken from a single Bi_2Se_3 nanowire. Three characteristic peaks are found at the position of 71 cm^{-1}, 131 cm^{-1}, and 171 cm^{-1}, which are related

to three vibrational modes of A^1_{1g}, E^1_g, and A^2_{1g}, respectively. This is consistent with the previous reports of the Bi_2Se_3 single crystal and nanostructures.[42–45]

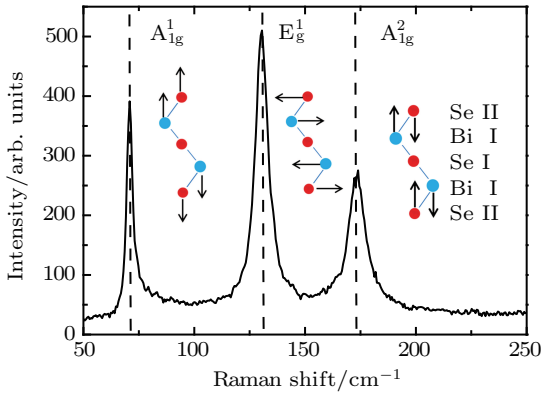


Fig. 4. (color online) Raman spectrum of a single nanowire.

The SEM image of a typical nanowire device is shown in Fig. 5(a). The width and thickness of the nanowire are about 130 nm and 21 nm, which are estimated by SEM and atomic force microscope (AFM), respectively, as shown in the insets of Fig. 5(a). Figure 5(b) shows the temperature-dependent resistance curve of the nanowire device, which suggests a metallic behavior. As shown by the above chemical composition analysis, there are Se vacancies in our nanowires, which may lead to the metallic behavior.[14,16] The four-terminal magnetoresistance was measured on a 9 T Quantum Design PPMS system. The magnetoresistance curve of the nanowire under vertical magnetic fields at 2 K is shown in Fig. 5(c). The weak anti-localization effect (WAL) with a sharp cusp is visible near the zero magnetic field, which is due to the spin–orbit coupling (SOC) effect or the surface states in Bi_2Se_3.[16,46] Under the parallel magnetic field along the longitudinal direction of nanowire at 2 K, the magnetoresistance curve is shown in Fig. 5(d). The WAL cusp near the zero magnetic field comes from the SOC of the bulk. At low magnetic fields, the pronounced and reproducible periodic resistance oscillations with a period of $\Delta B = 1.8$ T can be observed clearly, which is attributed to the AB oscillation.[16,28,47–49] The left inset in Fig. 5(d) shows the index dependence of oscillation minima of the field positions, and the period of magnetic field ($\Delta B = 1.8$ T) is obtained from the slope of the fitting straight line. The AB oscillation is caused by the quantum interference effects of phase coherent conduction electrons after completing closed trajectories which encircle a certain magnetic flux. The characteristic period of the external magnetic field could be described by $\Delta B = \Phi_0/S$, where the flux quantum $\Phi_0 = h/e$, h is Planck's constant, e is the electron charge, and S is the cross-sectional area of the nanowire. Considering our sample, the width and thickness of the nanowire are 130 nm and 21 nm, respectively, giving a cross-sectional area of about

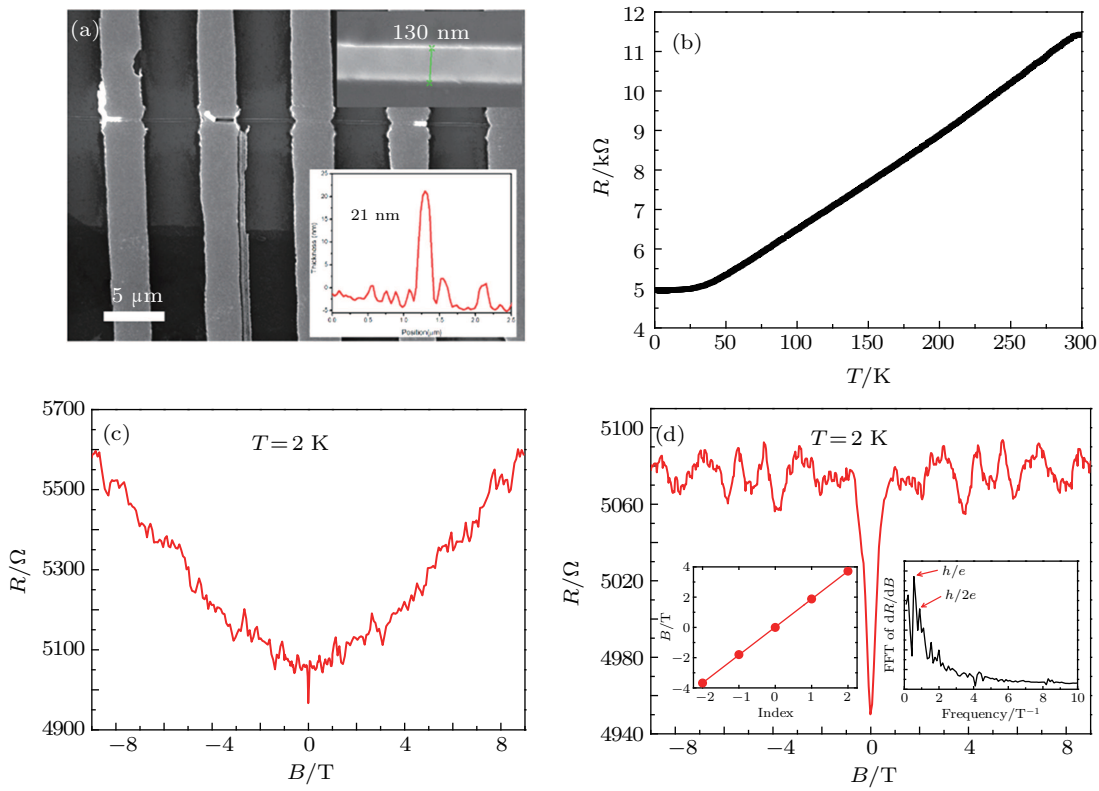


Fig. 5. (color online) Magnetoresistance properties of a single Bi_2Se_3 nanodevice. (a) SEM image of the Bi_2Se_3 nanodevice. The magnified SEM image and the AFM height diagram of the nanodevice are shown in the insets. (b) Temperature-dependent resistance curve at zero magnetic field. (c) Magnetoresistance curve in the vertical magnetic field at 2 K. (d) Magnetoresistance curve in the parallel magnetic field at 2 K. The magnetic field positions of resistance oscillation minima versus oscillation index at 2 K and the FFT of the dR/dB in −9 T to 9 T range are shown in the insets.

2.6×10^{-15} m^2, which is close to the estimated cross-sectional area $S = \Phi_0/\Delta B = 2.3 \times 10^{-15}$ m^2. The fast Fourier transform (FFT) of magnetoresistance derivative $\mathrm{d}R/\mathrm{d}B$ is shown in the right inset of Fig. 5(d). In addition to the prominent h/e oscillation of the AB effect, the oscillation frequency of $h/2e$ can also be observed, which is identified as the Altshuler–Aronov–Spival (AAS) effect that originates from WAL.[50] Compared with the AB effect, the AAS effect is more robust against temperature, which has been observed and analyzed in a previous report.[51] The observation of the AB oscillation in Bi_2Se_3 nanowire provides evidence of the existence of surface states of topological insulators. Actually, in our metallic nanowires, bulk carriers contribute to a significant portion in the electron transport. However, the phase coherence of surface states cannot be destroyed by the interaction between bulk and surface electrons, which suggests that the low-dimensional system is an ideal platform to explore the topological surface states of TI materials.

4. Conclusion

In conclusion, Bi_2Se_3 nanowires have been synthesized through a VLS process. The good crystallinity of the nanowires is characterized by HRTEM, XPS, and Raman spectra. The analysis of the chemical composition reveals the existence of Se vacancies in our nanowires. Magnetotransport measurements show the AB effect, manifesting the surface state nature of Bi_2Se_3 nanowires. Our results are helpful for understanding the growth mechanism and magnetoresistance properties of the single Bi_2Se_3 nanowire.

References

[1] Fu L, Kane C L and Mele E J 2007 *Phys. Rev. Lett.* **98** 106803
[2] Kane C L and Mele E J 2005 *Phys. Rev. Lett.* **95** 226801
[3] Koenig M, Wiedmann S, Bruene C, Roth A, Buhmann H, Molenkamp L W, Qi X L and Zhang S C 2007 *Science* **318** 766
[4] Moore J E and Balents L 2007 *Phys. Rev. B* **75** 121306
[5] Fu L and Kane C L 2007 *Phys. Rev. B* **76** 045302
[6] Chen Y L, Analytis J G, Chu J H, Liu Z K, Mo S K, Qi X L, Zhang H J, Lu D H, Dai X, Fang Z, Zhang S C, Fisher I R, Hussain Z and Shen Z X 2009 *Science* **325** 178
[7] Takagaki Y, Jenichen B, Jahn U, Ramsteiner M and Friedland K J 2012 *Phys. Rev. B* **85** 115314
[8] Qi X L, Hughes T L and Zhang S C 2008 *Phys. Rev. B* **78** 195424
[9] Qi X L, Li R D, Zang J D and Zhang S C 2009 *Science* **323** 1184
[10] Fu L and Kane C L 2008 *Phys. Rev. Lett.* **100** 096407
[11] Zhang J Y, Zhao B, Zhou T and Yang Z Q 2016 *Chin. Phys. B* **25** 117308
[12] He K, Ma X C, Chen X, Li L, Wang Y Y and Xue Q K 2013 *Chin. Phys. B* **22** 67305
[13] Chang C Z, Zhang J, Feng X, Shen J, Zhang Z, Guo M, Li K, Ou Y, Wei P, Wang L L, Ji Z Q, Feng Y, Ji S, Chen X, Jia J, Dai X, Fang Z, Zhang S C, He K, Wang Y, Lu L, Ma X C and Xue Q K 2013 *Science* **340** 167
[14] Pan H, Zhang K, Wei Z, Wang J, Han M, Song F, Wang X, Wang B and Zhang R 2017 *Appl. Phys. Lett.* **110** 053108
[15] Dufouleur J, Veyrat L, Teichgräber A, Neuhaus S, Nowka C, Hampel S, Cayssol J, Schumann J, Eichler B, Schmidt O G, Büchner B and Giraud R 2013 *Phys. Rev. Lett.* **110** 186806
[16] Peng H, Lai K, Kong D, Meister S, Chen Y, Qi X L, Zhang S C, Shen Z X and Cui Y 2010 *Nat. Mater.* **9** 225
[17] Qu F, Yang F, Chen J, Shen J, Ding Y, Lu J, Song Y, Yang H, Liu G, Fan J, Li Y, Ji Z, Yang C and Lu L 2011 *Phys. Rev. Lett.* **107** 016802
[18] Yan Y, Liao Z M, Zhou Y B, Wu H C, Bie Y Q, Chen J J, Meng J, Wu X S and Yu D P 2013 *Sci. Rep.* **3** 1264
[19] Lu H Z and Shen S Q 2016 *Chin. Phys. B* **25** 117202
[20] Checkelsky J G, Hor Y S, Liu M H, Qu D X, Cava R J and Ong N P 2009 *Phys. Rev. Lett.* **103** 246601
[21] Eto K, Ren Z, Taskin A A, Segawa K and Ando Y 2010 *Phys. Rev. B* **81** 195309
[22] Wang L X, Yan Y, Zhang L, Liao Z M, Wu H C and Yu D P 2015 *Nanoscale* **7** 16687
[23] Liu Y, Ma Z, Zhao Y F, Singh M and Wang J 2013 *Chin. Phys. B* **22** 67302
[24] Cho S, Kim D, Syers P, Butch N P, Paglione J and Fuhrer M S 2012 *Nano Lett.* **12** 469
[25] Kong D, Randel J C, Peng H, Cha J J, Meister S, Lai K, Chen Y, Shen Z X, Manoharan H C and Cui Y 2010 *Nano Lett.* **10** 329
[26] Cha J J, Claassen M, Kong D, Hong S S, Koski K J, Qi X L and Cui Y 2012 *Nano Lett.* **12** 4355
[27] Xiu F, He L, Wang Y, Cheng L, Chang L T, Lang M, Huang G, Kou X, Zhou Y, Jiang X, Chen Z, Zou J, Shailos A and Wang K L 2011 *Nat. Nano* **6** 216
[28] Lee S, In J, Yoo Y, Jo Y, Park Y C, Kim H J, Koo H C, Kim J, Kim B and Wang K L 2012 *Nano Lett.* **12** 4194
[29] Safdar M, Wang Q, Mirza M, Wang Z, Xu K and He J 2013 *Nano Lett.* **13** 5344
[30] Hamdou B, Gooth J, Dorn A, Pippel E and Nielsch K 2013 *Appl. Phys. Lett.* **103** 193107
[31] Li Z, Chen T, Pan H, Song F, Wang B, Han J, Qin Y, Wang X, Zhang R, Wan J, Xing D and Wang G 2012 *Sci. Rep.* **2** 595
[32] Wei Q, Su Y, Yang C J, Liu Z G, Xu H N, Xia Y D and Yin J 2011 *J. Mater. Sci.* **46** 2267
[33] Scanlon D O, King P D C, Singh R P, de la Torre A, Walker S M, Balakrishnan G, Baumberger F and Catlow C R A 2012 *Adv. Mater.* **24** 2154
[34] Ren Z, Taskin A A, Sasaki S, Segawa K and Ando Y 2011 *Phys. Rev. B* **84** 075316
[35] Kratzer P, Sakong S and Pankoke V 2012 *Nano Lett.* **12** 943
[36] Dubrovskii V G and Sibirev N V 2008 *Phys. Rev. B* **77** 035414
[37] Dubrovskii V G, Sibirev N V, Harmand J C and Glas F 2008 *Phys. Rev. B* **78** 235301
[38] Hamdou B, Kimling J, Dorn A, Pippel E, Rostek R, Woias P and Nielsch K 2013 *Adv. Mater.* **25** 239
[39] Givargizov E I 1975 *J. Cryst. Growth* **31** 20
[40] Milewski J V, Gac F D, Petrovic J J and Skaggs S R 1985 *J. Mater. Sci.* **20** 1160
[41] Mlack J T, Rahman A, Johns G L, Livi K J T and Marković N 2013 *Appl. Phys. Lett.* **102** 193108
[42] Zhang G, Qin H, Teng J, Guo J, Guo Q, Dai X, Fang Z and Wu K 2009 *Appl. Phys. Lett.* **95** 053114
[43] Yan Y, Zhou X, Jin H, Li C Z, Ke X, Van Tendeloo G, Liu K, Yu D, Dressel M and Liao Z M 2015 *Acs Nano* **9** 10244
[44] Richter W and Becker C R 1977 *Phys. Status Solidi B* **84** 619
[45] Zhang J, Peng Z, Soni A, Zhao Y, Xiong Y, Peng B, Wang J, Dresselhaus M S and Xiong Q 2011 *Nano Lett.* **11** 2407
[46] Huber T E, Celestine K and Graf M J 2003 *Phys. Rev. B* **67** 245317
[47] Zhang Y and Vishwanath A 2010 *Phys. Rev. Lett.* **105** 206601
[48] Fu Z G, Zhang P and Li S S 2011 *Appl. Phys. Lett.* **99** 243110
[49] Jens H B and Joel E M 2013 *Rep. Prog. Phys.* **76** 056501
[50] Bardarson J H, Brouwer P W and Moore J E 2010 *Phys. Rev. Lett.* **105** 156803
[51] Wang L X, Li C Z, Yu D P and Liao Z M 2016 *Nat. Commun.* **7** 10769